Supporting Information for

Regulating KBBF-like Structures via Charge-Assisted Hydrogen-Bonded Framework to Enable Easily Grown Ultraviolet Nonlinear Optical Crystal

Mingshu Zhang, [a] Shuya Zhao, [a] Zhen-Cheng Wu, [b] Yue Yin, [a] Zheyu Zhang, [a] Jiafeng Chen, [a] Sheng-Ping Guo, *[b] and Yan Zhou *[a]

[a] School of Chemical Science and Technology, Yunnan University, Kunming, Yunnan 650500, P. R. China

[b] Yunnan Key Laboratory of Electromagnetic Materials and Devices, School of Materials and Energy, Yunnan University, Kunming, Yunnan 650500, P. R. China

* Sheng-Ping Guo: spguo@ynu.edu.cn; Yan Zhou: yanzhou@ynu.edu.cn.

Contents

1. Experimental Section 3

2. Computational Method 5

3. Figures and tables. 7

3.1 Figures. 7

Fig. S1 Element mapping diagram and EDS of single-crystal SAN. 7

Fig. S2 Calculated (cal.) and experimental (exp.) powder XRD patterns of SAN. 7

Fig. S3 The transmittance spectrum in the 200–400 nm range of SAN. 8

Fig. S4 The IR spectrum of SAN. 8

Fig. S5 The contributions of $[C_6H_9N_2O_2S]$ and $[NO_3]$ to each SHG coefficient. 9

Fig. S6 The unit-sphere representation of the hyperpolarizability of $[C_6H_9N_2O_2S]$ and its packing orientation within the structure. 9

Fig. S7 The phase-matching cutoff edge of SAN. 10

3.2 Tables. 11

Table S1 Crystal data and structure refinement results for SAN. 11

Table S2 Fractional atomic coordinates ($\times 10^4$) and equivalent isotropic displacement parameters ($Å^2 \times 10^3$) for SAN. 12

Table S3 Selected distances (Å) for SAN. 13

4. References 14

1. Experimental Section

Reagent. All the reagents required for crystal growth were purchased from commercial sources and used without further purification: Sulfanilamide (99%), nitric acid (69%).

Synthesis and crystal growth. 0.86 g of sulfanilamide and 0.35 mL of nitric acid were added to 10 mL of deionized water and stirred until complete dissolution, followed by continued stirring for an additional hour to ensure homogeneity. The resulting solution was then transferred to a dry and well-ventilated environment and allowed to stand undisturbed for crystallization. After one week, centimeter-sized, colorless, block-shaped single crystals of SAN were obtained. The yield was calculated based on sulfanilamide and was approximately 85%. Notably, when the experiment was repeated using beakers of different diameters, the size of the as-grown SAN single crystals varied with the container diameter. This correlation indicates that SAN exhibits favorable crystal growth habit.

Single−Crystal X−ray Diffraction (SCXRD). The crystallographic data of SAN were obtained at 293 K by means of a Rigaku FR-X microfocus diffractometer (45 kV, 66 mA) equipped with a graphite monochromator (Mo−$K\alpha$ radiation, λ = 0.71073 Å). The collection and processing of diffraction data were executed using CrysAlisPro software,[1] and the refinement was conducted via the full−matrix least−squares method on F^2 with the Olex2-1.5 program package.[2] Eventually, the final structure was verified through the PLATON program to confirm the non-existence of higher symmetry.[3] Hydrogen atoms were placed in calculated positions and refined using riding/rotating-group models (AFIX 43 for C-H and AFIX 137 for the N2-bound H atoms), with Uiso(H)=1.2Ueq of the parent atoms.

Powder X−ray Diffraction (PXRD). The powder sample of SAN was analyzed through a Rigaku TTRIII-18KW powder diffractometer with Cu-$K\alpha$ radiation at room temperature. The 2ϑ scanning range was from 5° to 65°, with a step size of 0.02°. The powder XRD pattern obtained experimentally was compared with that calculated based on CIF file to verify the purity of the sample being tested.

Energy dispersive X−ray spectroscopy (EDS). Elemental analysis of SAN crystals was performed with a FEI Nova NanoSEM 450 scanning electron microscope equipped with an energy dispersive X-ray spectrometer. The resulting elemental analysis results demonstrate

compatibility with the elemental stoichiometry ratios obtained through refinement of the single crystal diffraction data: C : N : O : S = 7.51 : 3.25 : 4.80 : 1 (**Fig. S1**).

UV−Vis−NIR Diffuse Reflectance Spectroscopy. The diffuse reflectance spectrum of SAN was acquired at room temperature through the utilization of the PerkinElmer Lambda 900 spectrophotometer within the wavelength range spanning from 200 to 800 nm.

Fourier Transform Infrared (FT-IR) Spectroscopy. The sample for IR measurements was prepared by thoroughly mixing and grinding SAN powder with dry spectroscopic-grade KBr at a mass ratio of 1 : 200, followed by pressing into a pellet. The infrared spectrum of SAN was obtained at room temperature in the wavenumber range from 400 to 4000 cm^{-1} with the Nicolet iS10 Fourier transform infrared spectrometer.

The characteristic peaks at 3365 and 3199 cm^{-1} are attributed to the ν(N-H) vibrations of the amino and sulfonamide groups, while the peak at 2923 cm^{-1} corresponds to ν(C-H) of the aromatic ring. The peak at 2577 cm^{-1} is assigned to strongly hydrogen-bonded ν(N-H). The bands located at 1629 and 1599 cm−1 are mainly attributed to ν(C=C) of the aromatic skeleton coupled with δ(N-H), and the peaks at 1537, 1523, and 1498 cm^{-1} are assigned to aromatic skeletal vibrations with contributions from δ(N-H). The intense peaks at 1311 and 1156 cm^{-1} correspond to ν(SO_2). The nitrate anion is evidenced by the strong peak at 1388 cm^{-1} assigned to ν(NO^{3-}), while the peaks in the 1094–1031 cm^{-1} region (1094, 1048, and 1031 cm−1) are attributed to nitrate-related ν(N-O) modes overlapped with ν(C-N)/ν(S-N). The peaks at 915, 844, and 819 cm^{-1} are assigned to γ(C-H) vibrations of the substituted benzene ring (with 844 and 819 cm^{-1} characteristics of a para-disubstituted ring), whereas the peaks at 692 and 669 cm^{-1} correspond to δ(NO^{3-}) coupled with aromatic γ modes. The low-frequency peaks at 540 cm^{-1} are attributed to δ(SO_2), and those at 484 and 460 cm^{-1} are assigned to framework vibrations involving ν(C−S)/ν(S−N). (δ, ν, γ, and β stand for bending vibration, stretching vibrations, out-of-plane and in-plane bending vibration, respectively).

Thermogravimetric (TG) and Derivative thermogravimetric (DTG) analyses. The TG and DTG data of SAN were obtained by a Metter Toledo synchronous differential thermal analyzer with a temperature range of 30−800°C and a heating rate of 10°C/min under an argon atmosphere.

Second−Harmonic Generation (SHG) Measurement. By employing the modified Kurtz-Perry method,[4] the SHG response of SAN was assessed under the irradiation of 1064 nm laser at a

pulse energy of 1 mJ. The crystals of SAN and the standard KH_2PO_4 (KDP) were ground and then sieved into five groups with particle size ranges of 30−50 μm, 50−75 μm, 75−100 μm, 100−150 μm, and 150−200 μm respectively, for conducting the phase−matching tests. The DU420A-BR-DD charge-coupled device (CCD) camera was used to detect and record the SHG signals at 532 nm.

Birefringence Measurement. The birefringence of SAN was measured under a 546 nm light source by employing a Zeiss Axio Scope A5 microscope equipped with the Berek compensator. The birefringence (Δn) was calculated using the formula $R = \Delta n \times T$, where R stands for the optical path difference and T represents the thickness of the crystal under test.

2. Computational Method

Bravais-Friedel-Donnay-Harker (BFDH) model simulation. The simulation of the crystal habit of SAN was carried out using the BFDH model.[5]

Hirshfeld surface analysis. The hydrogen atom positions in the SAN structure used for Hirshfeld surface analysis were first optimized using the CP2K program at the PBE-D4/6-31G** level.[6] The optimized geometry was then processed with Multiwfn 3.8(dev) code to perform cluster extraction and subsequent Hirshfeld surface analysis. Isosurface visualizations of the Hirshfeld surfaces were generated using VMD 1.9.3 program,[7] while fingerprint plots and quantitative data on intermolecular contact areas were computed and exported directly from Multiwfn 3.8(dev).

Independent Gradient Model based on Hirshfeld partition (IGMH). Cluster extraction of the SAN structure was first carried out using Multiwfn 3.8(dev). The resulting structural models were then subjected to hydrogen atom position optimization employing Gaussian 16 at the B3LYP/6-31G* level,[8] with inclusion of DFT-D3(BJ) dispersion correction. The resultant wave function files were subsequently used for IGMH analysis within the Multiwfn 3.8(dev). The visualization processing of the calculation results is conducted using the VMD 1.9.3 program.

Polarizability anisotropy and hyperpolarizability calculation. The polarizability anisotropy and hyperpolarizability of $[C_6H_9N_2O_2S]$, $[BeO_3F]$ and $[BO_3]$ groups were computed by means of Gaussian 16 under the B3LYP/def2-TZVP condition, and the results were post-processed using the Multiwfn 3.8(dev) code.

Molecular orbitals and 3D ELF diagrams. The molecular orbitals and 3D ELF maps of SAN were

computed using CP2K software. Molecular orbital calculations grounded in time-dependent density functional theory (TDDFT) were conducted at the PBE/TZVP-GTH level; 3D ELF calculation was performed at the PBE/DZVP-MOLOPT-SR-GTH level. The visualization of the calculation results is presented by the VESTA program.

Electronic band structure and density of states (DOS). The theoretical calculations of the band structure and DOS of SAN were performed using the CASTEP module. The Perdew-Burke-Ernzerhof (PBE) parametrization within the generalized gradient approximation (GGA) was selected as the exchange-correlation functional.[9] The valence electrons of each atom in SAN were considered as H-1s^1, C-2$s^2$2p^2, N-2$s^2$2p^3, O-2$s^2$2p^4 and S-3$s^2$3p^4, respectively. The cutoff energy was set at 750 eV and the Monkhorst-Pack *k*-point grid for the Brillouin zone was set as 3 × 3 × 3.

Linear and nonlinear optical properties. The theoretical computations of the linear and nonlinear optical properties of SAN were based on the ABINIT program.[10] The linear optical properties are characterized by the complex dielectric function $\varepsilon = \varepsilon_{re}(\omega) + i\varepsilon_{im}(\omega)$, where $\varepsilon_{re}(\omega)$ and $\varepsilon_{im}(\omega)$ respectively stand for the real and imaginary parts of the dielectric function. $\varepsilon_{im}(\omega)$ can be calculated in line with the formula $\frac{4\pi}{\Omega}\sum_{nmk} f_{nm}(k)\frac{r^{i}_{nm}(k)r^{j}_{mn}(k)}{\omega_{mn}(k)-\omega} + \delta_{ij}$, where $r^{i}_{nm}(k)$ represents the position matrix element between states *m* and *n*; $\varepsilon_{re}(\omega)$ can be derived from $\varepsilon_{im}(\omega)$ through the Kramers−Kroning transformation. Based on this, the refractive index (*n*) can be further obtained by employing the formula $n(\omega) = \sqrt{\frac{\sqrt{\varepsilon^2_{re}(\omega) + \varepsilon^2_{im}(\omega)} + \varepsilon_{re}(\omega)}{2}}$. The frequency-dependent second-order nonlinear susceptibility tensor $\chi_{ijk}(2\omega,\omega,\omega)$ is computed based on density functional perturbation theory and Sharma's sum formalism.[11]

3. Figures and tables.

3.1 Figures.

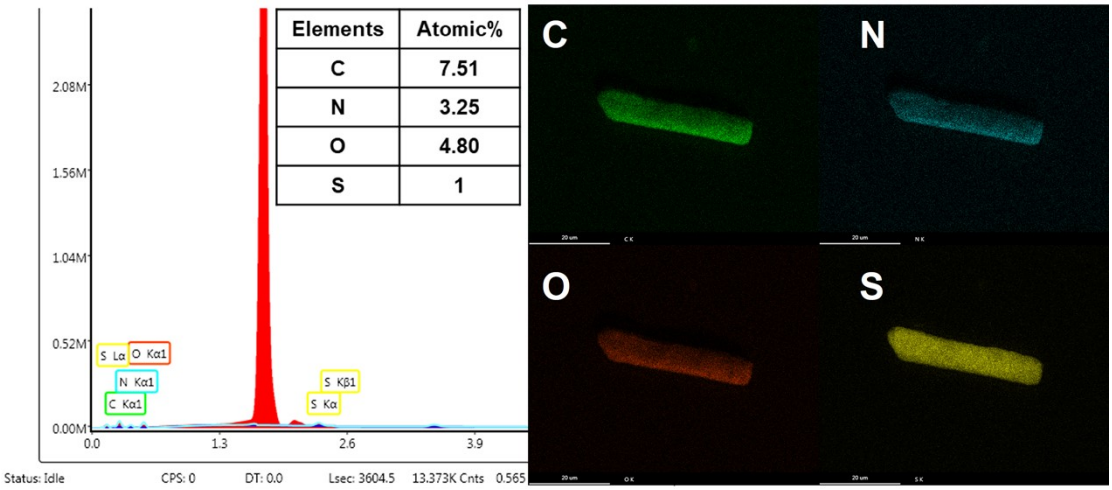

Fig. S1 Element mapping diagram and EDS of single-crystal SAN.

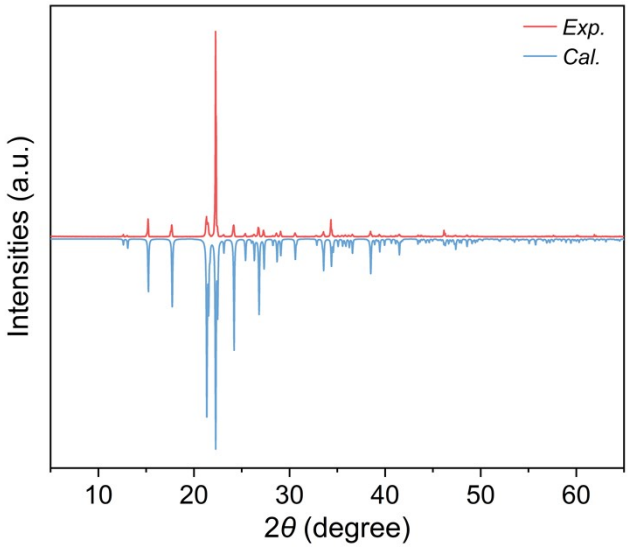

Fig. S2 Calculated (cal.) and experimental (exp.) powder XRD patterns of SAN.

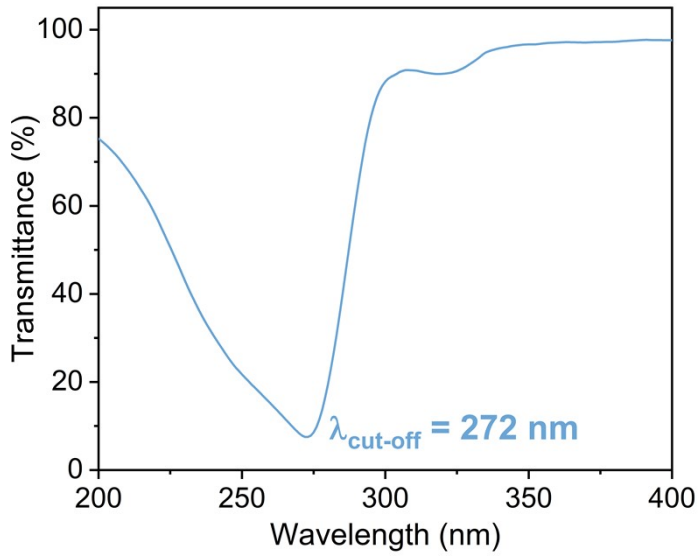

Fig. S3 The transmittance spectrum in the 200–400 nm range of SAN.

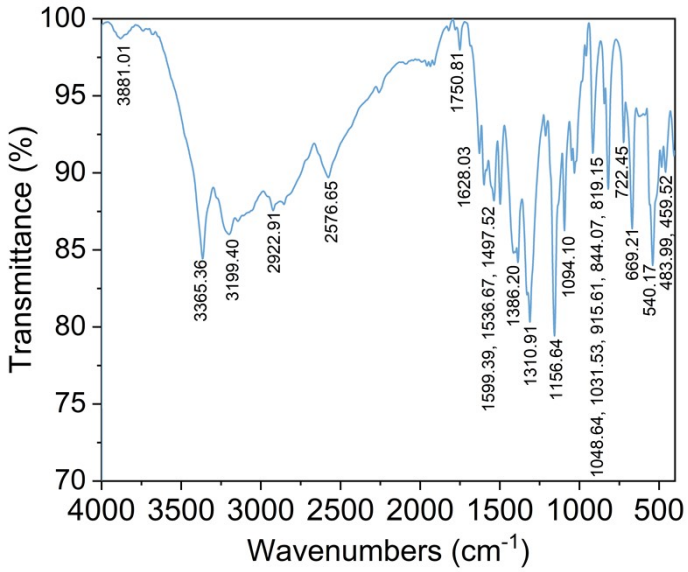

Fig. S4 The IR spectrum of SAN.

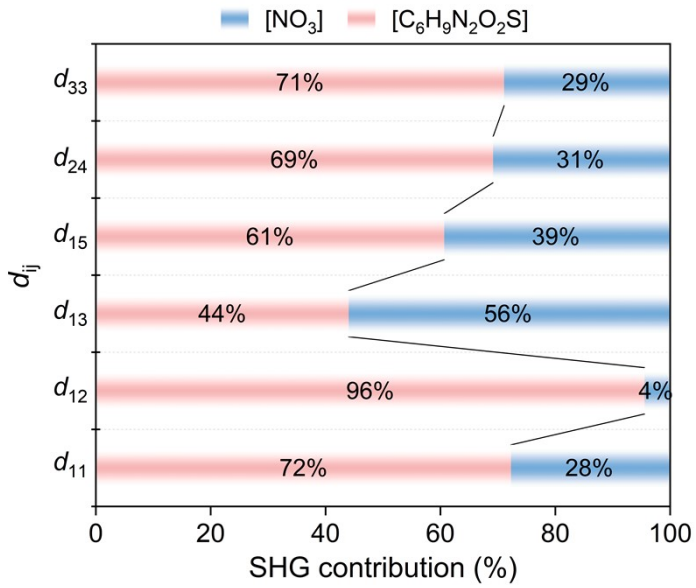

Fig. S5 The contributions of $[C_6H_9N_2O_2S]$ and $[NO_3]$ to each SHG coefficient.

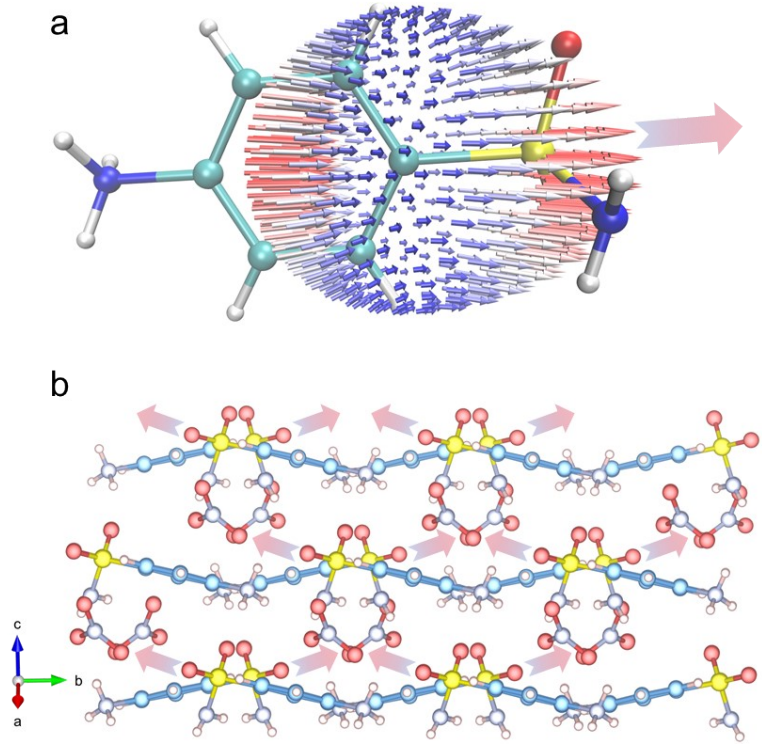

Fig. S6 The unit-sphere representation of the hyperpolarizability of $[C_6H_9N_2O_2S]$ and its packing orientation within the structure.

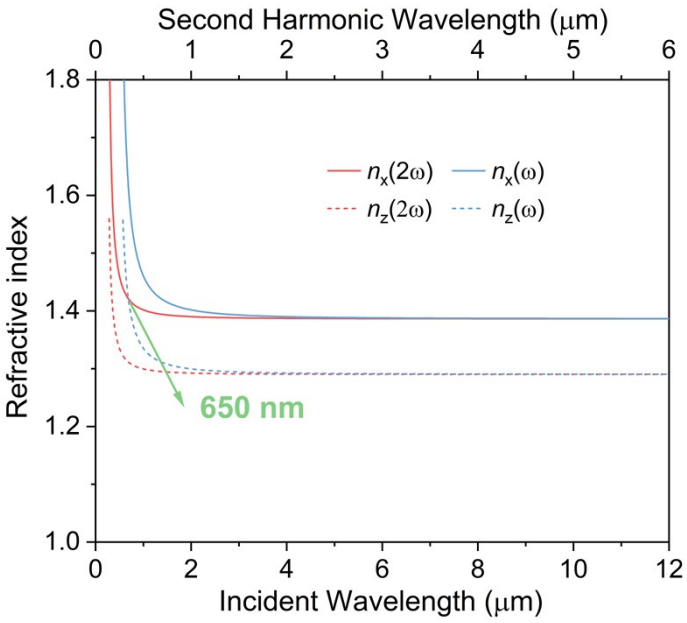

Fig. S7 The phase-matching cutoff edge of SAN.

3.2 Tables.

Table S1 Crystal data and structure refinement results for SAN.

Empirical formula	$C_6H_9N_2SO_2{\cdot}NO_3$
CCDC Number	2502321
Fw	235.22
Temperature (K)	300.5(7)
Space group	*Cc*
a (Å)	14.1524(8)
b (Å)	8.1924(4)
c (Å)	8.6986(5)
α (°)	90
β (°)	107.039(6)
γ (°)	90
Volume (Å^3)	964.26(10)
Z	4
D_{calcd} (g·cm^{-3})	1.620
μ (mm^{-1})	0.343
GOF on F^2	1.070
$R_1{}^a$ ($I > 2\sigma(I)$)	0.0237
$wR_2{}^b$ ($I > 2\sigma(I)$)	0.0625
$R_1{}^a$ (all data)	0.0244
$wR_2{}^b$ (all data)	0.0629
Flack	0.006(19)
$\Delta\rho_{max}/\Delta\rho_{min}$ (e Å^{-3})	0.17/–0.14

$^aR = \Sigma||F_o|-|F_c||/\Sigma|F_o|$, $^bwR = (\Sigma(w(F_o^2-F_c^2)^2)/\Sigma(w(F_o^2)^2))^{1/2}$.

Table S2 Fractional atomic coordinates (× 10^4) and equivalent isotropic displacement parameters (Å^2 × 10^3) for SAN.

Atom	*x*	*y*	*z*	*U*(eq)
C1	2651.3(14)	1367(2)	2314(2)	31.3(4)
C2	3604.7(15)	1349(2)	3343(3)	38.0(4)
C3	4135.7(14)	−103(3)	3573(3)	39.9(4)
C4	3700.0(14)	−1488(2)	2779(2)	30.3(4)
C5	2743.1(16)	−1485(2)	1770(3)	38.8(4)
C6	2214.0(15)	−39(3)	1529(3)	39.6(4)
N1	1715.6(18)	3709(3)	156(3)	48.0(5)
N2	4271.5(13)	−3000(2)	3034(2)	34.4(3)
N3	5037.5(14)	3523(2)	1986(3)	42.0(4)
O1	5447.6(16)	2385(2)	1507(3)	62.5(5)
O2	1044.3(14)	2863(2)	2291(3)	56.7(5)
O3	4316.1(13)	4247(2)	1013.6(19)	49.6(4)
O4	2593.8(13)	4454(2)	2932(2)	49.4(4)
O5	5317.4(14)	3974(2)	3413(2)	53.1(4)
S1	1967.5(3)	3208.5(5)	2003.2(4)	33.72(13)
H1A	1370(20)	2990(40)	−340(40)	58
H1B	2210(20)	4100(40)	−80(40)	58
H2A	3985	−3715	2268	41
H2B	4296	−3415	3990	41
H2C	4882	−2794	2998	41
H2	3886	2295	3873	46
H3	4779	−138	4255	48
H5	2459	−2439	1259	47
H6	1571	−9	848	48

Table S3 Selected distances (Å) for SAN.

Bond	Distances	Bond	Distances
C1−C2	1.383(3)	C5−C6	1.384(3)
C1−C6	1.388(3)	N3−O1	1.233(3)
C1−S1	1.7700(19)	N3−O3	1.267(3)
C3−C2	1.390(3)	N3−O5	1.244(3)
C4−C3	1.377(3)	S1−N1	1.594(2)
C4−C5	1.381(3)	S1−O2	1.4287(16)
C4−N2	1.460(2)	S1−O4	1.4352(17)

4. References

1 Rigaku Oxford Diffraction, CrysAlisPro Software system, version v42.69a, Rigaku Corporation, Oxford (UK), 2022.

2 O. V. Dolomanov, L. J. Bourhis, R. J. Gildea, J. A. K. Howard and H. Puschmann, *J. Appl. Cryst.*, 2009, 42, 339−341.

3 A. L. Spek, PLATON, a Multipurpose Crystallographic Tool, Utrecht University, Utrecht (Netherlands), 2005.

4 S. K. Kurtz and T. T. Perry, *J. Appl. Phys.*, 1968, **39**, 3798−3813.

5 R. Docherty, G. Clydesdale, K. J. Roberts and P. Bennema, *J. Phys. D: Appl. Phys.*, 1991, **24**, 89.

6 D. K. Thomas, I. Marcella, D. B. Mauro, V. R. Vladimir, S. Patrick, S. Frederick, L. Teodoro, Z. K. Rustam, S. Ole, S. Florian, G. Dorothea, W. Jan, C. Sergey, H. B.-H. Mohammad, W. Valéry, B. Urban, T. Mathieu, S. J. Alice, L. Alfio, P. Hans, M. Tiziano, S. Robert, G. Manuel, A. Samuel, H. Nico, K. S. Gregory, H. Anna, B. Augustin, B. Fabian, T. Gloria, G. Andreas, L. Michael, B. Iain, J. M. Christopher, P. Christian, W. Matt, V. Joost, K. Matthias and H. Jürg, *J. Chem. Phys.*, 2020, **152**, 194103.

7 W. Humphrey, A. Dalke and K. Schulten, *J. Mol. Graphics*, 1996, **14**, 33−38.

8 M. J. Frisch, G. W. Trucks, H. B. Schlegel, G. E. Scuseria, M. A. Robb, J. R. Cheeseman, G. Scalmani, V. Barone, G. A. Petersson, H. Nakatsuji, X. Li, M. Caricato, A. V. Marenich, J. Bloino, B. G. Janesko, R. Gomperts, B. Mennucci, H. P. Hratchian, J. V. Ortiz, A. F. Izmaylov, J. L. Sonnenberg, D. Williams-Young, F. Ding, F. Lipparini, F. Egidi, J. Goings, B. Peng, A. Petrone, T. Henderson, D. Ranasinghe, V. G. Zakrzewski, J. Gao, N. Rega, G. Zheng, W. Liang, M. Hada, M. Ehara, K. Toyota, R. Fukuda, J. Hasegawa, M. Ishida, T. Nakajima, Y. Honda, O. Kitao, H. Nakai, T. Vreven, K. Throssell, J. A. Montgomery, Jr., J. E. Peralta, F. Ogliaro, M. J. Bearpark, J. J. Heyd, E. N. Brothers, K. N. Kudin, V. N. Staroverov, T. A. Keith, R. Kobayashi, J. Normand, K. Raghavachari, A. P. Rendell, J. C. Burant, S. S. Iyengar, J. Tomasi, M. Cossi, J. M. Millam, M. Klene, C. Adamo, R. Cammi, J. W. Ochterski, R. L. Martin, K. Morokuma, O. Farkas, J. B. Foresman and D. J. Fox, Gaussian 16, Revision B.01, Gaussian, Inc., Wallingford CT, 2016.

9 J. P. Perdew, J. A. Chevary, S. H. Vosko, K. A. Jackson, M. R. Pederson, D. J. Singh and C. Fiolhais, *Phys. Rev. B*, 1992, **46**, 6671−6687.

10 X. Gonze, B. Amadon, G. Antonius, F. Arnardi, L. Baguet, J.-M. Beuken, J. Bieder, F. Bottin, J. Bouchet, E. Bousquet, N. Brouwer, F. Bruneval, G. Brunin, T. Cavignac, J.-B. Charraud, W. Chen, M. Côté, S. Cottenier, J. Denier, G. Geneste, P. Ghosez, M. Giantomassi, Y. Gillet, O. Gingras, D. R. Hamann, G. Hautier, X. He, N. Helbig, N. Holzwarth, Y. Jia, F. Jollet, W. Lafargue-Dit-Hauret, K. Lejaeghere, M. A. L. Marques, A. Martin, C. Martins, H. P. C. Miranda, F. Naccarato, K. Persson, G. Petretto, V. Planes, Y. Pouillon, S. Prokhorenko, F. Ricci, G.-M. Rignanese, A. H. Romero, M. M. Schmitt, M. Torrent, M. J. V. Setten, B. V. Troeye, M. J. Verstraete, G. Zérah and J. W. Zwanziger, *Comput. Phys. Commun.*, 2020, **248**, 107042.

11 S. Sharma, C and Ambrosch-Draxl, *Phys. Scr.*, 2004, **109**, 128.